ADVANCED SUSTAINABLE SYSTEMS
www.advsustainsys.com

# High Ionic Flux Sub-Micro Channels Membrane Model for Salinity Gradient Power Generation

*Jiaqiao Jiang, Bingxin Lu, Yanglei Xu, Jin Zhai,* and Xia Fan**

**Salinity gradient cells are widely used in power generation from gradient concentration solutions of one electrolyte. High ionic flux sub-micro channels membrane can offer a high current density for salinity gradient power generation with a significant power output. Herein, based on numerical simulation model with Poisson-Nernst-Planck-Navier-Stokes (PNP-NS) equations, a high ionic flux sub-micro channel model with assumption is introduced that measured current is contributed by $Cl^-$ ionic flux across the membrane. An ion channel system is built for experiment, in which a glass membrane with regular symmetric sub-micro cylindrical channels and high effective channel area is applied, ion conductance and salinity gradient energy conversion property are tested. This PNP-NS equations model simulation fits experiment well, its mechanism is also studied by the model. In addition, by mixing artificial sea water (0.5 M NaCl) and river water (0.01 mM NaCl), the output power density of this 50-fold salinity gradient system can achieve 4.16 W $m^{-2}$, and the highest output power density will be up to 7.91 W $m^{-2}$ under a 0.5 M/0.001 M 500-fold salinity gradient. This high ionic flux membrane shows a good performance for practical application in salinity gradient power generation.**

## 1. Introduction

Development of large reversible and sustainable clean energy demand urgent attention under the background of exploration of new energy sources.[1–3] Salinity gradient power, one of new types of energy sources that can be captured between water with different salinities partitioning by a membrane, has received widespread attention in recent years.[4–8] This energy can be captured from seawater and fresh water using techniques like pressure-retarded osmosis and reverse electrodialysis based on anion and cation exchange membrane.[8–14] When two fluids of different concentrations are located on bilateral sides of an ion-selective membrane, the mixed Gibbs free energy can push ion-selective directional movement to release as electric energy.[15,16] However, if reversing electroosmosis technology is to provide energy for industrial development, the power density of salt-to-water power generation should be at least 5.0 W $m^{-2}$, which is very challenging because most of ion-exchange membranes do not have sufficient ionic flux.[17] Thus, low ionic throughput limits further increase in power density. In recent researches, various heterostructure and homogeneous membrane materials are emerged, such as anodic alumina oxide (AAO), silica nanochannels, graphene oxide, carbon nitride, and various polymer materials.[18–36] They were used to prepare ion selective membranes, and the pore diameters are controlled below 100 nm in order to maintain a good membrane selectivity. As a result, the flux of ion transmembrane is limited, which is not beneficial to improve the performance of energy conversion. Therefore, exploring ion-selective membrane with high ionic flux is significant for salinity gradient power generation.

In this work, we introduced a numerical simulation model for salinity gradient power generation system with a high ionic flux ion channel. The model is still based on numerical simulation model of an ion channel with Poisson-Nernst-Planck-Navier-Stokes (PNP-NS) equations, while several complements to the assumption were used. For this high ionic flux system, we assumed that measured current is limited by $Cl^-$ ionic flux across the sub-micro channel, as the ionic flux across membrane was high enough and the output current occurs due to the reduction or oxidation reaction of $Cl^-$ on Ag/AgCl electrodes in NaCl solution. With this assumption, the redox potentials of salinity gradient system simulated from I-V characteristic curves by Poisson-Nernst-Planck (PNP) equations model would be corresponding to the results calculated by Nernst redox equations. Considering ion channel across membrane has charged surface, liquid fluid driven by electroosmosis is not neglectable and could be described by Navier-Stokes (NS) equations. In the experiment, an ion channel system with a special glass membrane has high porosity and regular symmetric sub-micro cylindrical channels was built. This membrane has a negative surface charge in

J. Jiang, B. Lu, J. Zhai, X. Fan
Key Laboratory of Bio-Inspired Smart Interfacial Science and Technology of Ministry of Education
School of Chemistry
Beihang University
Beijing 100191, P. R. China
E-mail: zhaijin@buaa.edu.cn; fanxia@buaa.edu.cn
Y. Xu
Beijing Key Laboratory of Lignocellulosic Chemistry
College of Materials Science and Technology
Beijing Forestry University
Beijing 100083, P. R. China

The ORCID identification number(s) for the author(s) of this article can be found under https://doi.org/10.1002/adsu.202300175

**DOI: 10.1002/adsu.202300175**

 

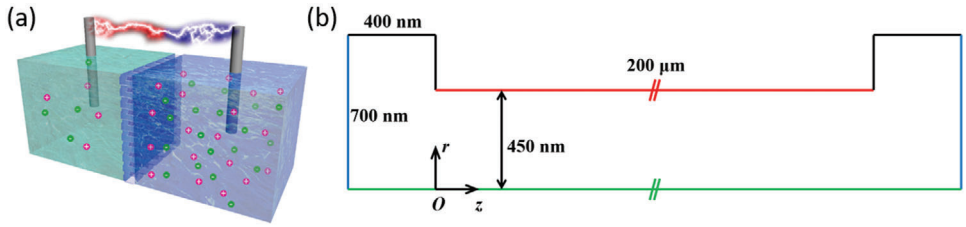


**Figure 1.** a) Schematic illustration of the energy harvesting process under a concentration gradient in glass channels membrane. b) Geometry of the 2D axisymmetric model. Detailed conditions of boundaries are in Figure S3 (Supporting Information).

neutral pH electrolyte aqua solution due to the presence of a large amount of Si-OH on the surface of glass channels. We tested its ion conductance and applied it for salinity gradient power generation, aiming to explore properties of sanity gradient energy capture from high ionic throughput.[37] In numerical simulations, ion conductance simulation could match experiment, indicates our model is reliable for this high ionic flux sub-micro glass channels membrane. We furtherly simulated *I*–*V* characteristic curves of 5-fold, 50-fold, and 500-fold salinity gradient systems, and discussed the relationship of diffusion flux, convection flux, and electrophoresis flux to ionic current by PNP-NS equations when the salinity gradient system outputting power. As a result, diffusion flux and convection flux are beneficial to the selectivity of cation while maintaining high throughput. Consequently, the high ionic flux membrane has a good performance on osmotic energy conversion. In addition, experimentally investigated the salinity gradient power generation with different NaCl concentration gradients, showing the maximum output power density of 7.91 W $m^{-2}$ under the 500-fold (0.001 M/0.5 M) salinity gradient. As artificial seawater (0.5 M NaCl) and river water (0.01 M NaCl)[28] were mixed, the value could still remain 4.16 W $m^{-2}$.

## 2. Result and Discussion

### 2.1. Numerical Model Building and Simulation Method of High Ionic Flux Sub-Micro Channel System

#### *2.1.1. Build of Poisson-Nernst-Planck-Navier-Stokes equations model*

To study the property of this high ionic flux sub-micro channel system with numerical simulation, according to the ion channel testing experiment device for salinity gradient power generation in **Figure 1**a, a model was built by 2D axisymmetric dimension method. As the geometry in Figure 1b, a cylindrical channel with 200 μm length and 450 nm radius rotating an axis was set as a sub-micro channel. Two buffering electrolyte reservoirs connected on both sides of channel were set as 400 nm thick and 700 nm in radius, so that the active area of section is about 41.3%, which is beneficial to increase osmotic energy conversion density in salinity gradient power generation and reduce membrane resistance. In our experiment device, a test area (recorded as $S_{test}$) of $3 \times 10^4$ $\mu m^2$ is usually used, so we could assume $2 \times 10^4$ active channels in parallel, and multiply this factor directly while comparing simulated currents with measured results.

A simple bare glass channel, which could possess negative surface charge in neutral pH electrolyte solution because of the deprotonation of hydroxyls. Negative surface charge of the glass channel could affect ion transportation. First, ionic transport properties are affected by electrostatic effects, which were attributed to the negative surface charge of glass channels.[39] In addition, considering the 900 nm diameter of glass channel, much longer than the Debye length of monovalent ion in aqua solution above 1 mM, hydrodynamics of liquid fluid cannot be neglect. Here, dynamics between the fluid and the charged channel surface can be described by electroosmosis under electrostatic field.

With hydrodynamics of liquid fluid introduced by electroosmosis in consideration, PNP-NS equations are required. Electrostatic field could be described by Poisson equation, containing external applied voltage, charged surface of channel, and ion in solution as electric charge. Ionic flux in solution could be described by Nernst-Planck equations. Here, ionic flux is consisted of diffusion flux, convection flux, and electrophoresis flux. Hydrodynamics of liquid fluid could be described by Navier-Stokes equations.[41–43] As liquid flows in this channel at a quite low rate, and the length of channel is much longer than its width, it could be assumed as laminar flow.[38] In this model, density variation by salt concentration is without consideration. Assumption of boundary conditions is similar as we used in previous works with several complements.[44–46] Besides analytic method, PNP-NS equations can be solved by several numerical methods, such as finite element method and dynamic density functional theory.[48–50] Here, finite element method numerical simulation was performed in commercial software COMSOL Multiphysics.

Numerical model of PNP-NS equations is described by Equations (1) to (5).

The electrical potential in space of model induced by ion concentration can be described by Poisson equation as Equation (1):

$$\nabla^2 \varphi = -\frac{F}{\epsilon} \sum z_i c_i,\ i = +, - \tag{1}$$

where $c_i$, $z_i$ are ion concentration, charge number of each ion species $i$. In this experiment, species + represents $Na^+$ cation, species – represents $Cl^-$ anion. $\varphi$ represents electrical potential. $F$ and $\epsilon$ represent Faraday constant and dielectric constant of aqua solution as $9.649 \times 10^4$ C $mol^{-1}$ and $6.906 \times 10^{-10}$ C $V^{-1}$ $m^{-1}$, or $\epsilon_r = 78$.

The flux density of each ion species in space of model can be described by Nernst-Planck equation as Equations (2) and (3):

$$\nabla \cdot \mathbf{J} = 0 \tag{2}$$

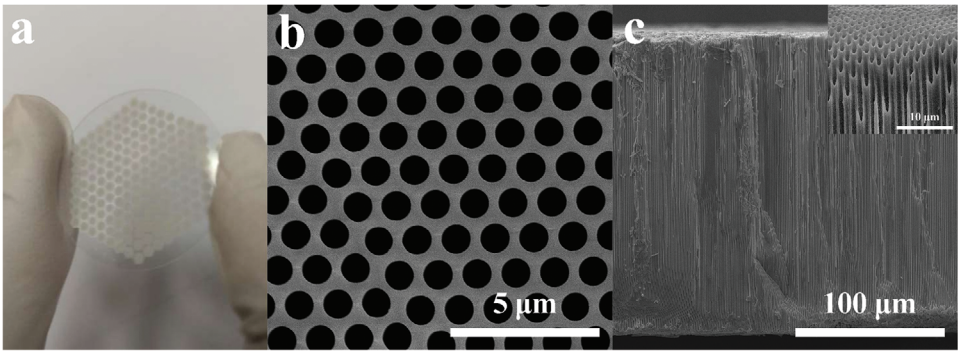


**Figure 2.** Photograph and scanning electron microscope (SEM) images of the glass membrane. a) Photograph of the glass membrane. b) SEM image of top view on glass nanochannels membrane, the diameter of one channel is ≈900 nm. c) SEM image of cross view on glass nanochannels membrane, the thickness of it is about 200 μm.

$$\mathbf{J}_i = -D_i \nabla c_i - \frac{F}{RT} D_i z_i c_i \nabla \varphi + c_i \mathbf{u},\ i = +, - \tag{3}$$

where $J$ and $D$ are ionic flux density and diffusion coefficient of ion, $D$- ($Cl^-$) and $D_+$ ($Na^+$) set in model are $2.03 \times 10^{-9}$ $m^2$ $s^{-1}$ and $1.33 \times 10^{-9}$ $m^2$ $s^{-1}$. u is velocity of fluid. $T$, is the absolute temperature and given as room temperature 293.15 K in model. $R$ represents universal gas constant as 8.314 J $mol^{-1}$ $K^{-1}$.

While without velocity of fluid in consideration, as $\boldsymbol{u} = 0$ in Equation (3), Equations (1) to (3) are the definition of Poisson-Nernst-Planck (PNP) equations.

Furtherly, hydrodynamics of liquid laminar flow in space of model could be described by Navier-Stokes equations as Equations (4) and (5):

$$\nabla \cdot \mathbf{u} = 0 \tag{4}$$

$$-\nabla p + \mu \nabla^2 \mathbf{u} - F \sum z_i c_i \nabla \varphi = 0,\ i = +, - \tag{5}$$

where $p$ is pressure of liquid, $\mu$ is dynamic viscosity of aqua solution as $0.9 \times 10^{-3}$ Pa s.

For glass channel, its charge density $\sigma_s$ and potential $\zeta_s$ on channel wall are important boundary conditions to PNP-NS equations.[51] For boundaries of channel charged surface (red lines in **Figure 2**b), we have Equations (6) and (7) to describe their boundary conditions:

$$\mathbf{n} \cdot \nabla \varphi = -\frac{\sigma_s}{\varepsilon} \tag{6}$$

$$\mathbf{u} = -\frac{\varepsilon \zeta_s}{\mu} \nabla \varphi \tag{7}$$

$\sigma_s$ and $\zeta_s$ would be analyzed in part 2.3. Other boundary conditions are described in SI.

The ionic flux of each ion species can be calculated from its density through a section vertical to axis. The ionic current should be represented by ionic flux along the axis, and the total current is a sum of ionic current of each ion species, as Equations (8) and (9):

$$I_{z,i} = F z_i \iint J_{z,i} ds,\ i = +, - \tag{8}$$

$$I_z = \sum I_{z,i},\ i = +, - \tag{9}$$

### *2.1.2. Measured Ion Current Assumption and I–V Curves Simulation of Salinity Gradient Redox Potentials Calculated by Nernst Redox Equations*

To study how the ionic current generates in this system, first, we know that with the presence of salinity concentration gradient, two reactions occur separately on electrodes of both sides in the cell could produce a redox potential ($E_{redox}$).[40] Here, we use a pair of Ag/AgCl electrodes as an example in salinity gradient system of NaCl aqua solution, so the non-transfer $E_{redox}$ is produced by Equation (10) following this redox reaction:

$$\begin{aligned} &-:\ Ag + Cl^-\left(c_H\right) \rightarrow AgCl + e^- \\ &+:\ AgCl + e^- \rightarrow Ag + Cl^-\left(c_L\right) \\ &\text{Redox reaction}: Cl^-\left(c_H\right) \rightarrow Cl^-\left(c_L\right) \end{aligned} \tag{10}$$

$E_{redox}$ is generated between the two Ag/AgCl electrodes and calculated by Equation (11) of Nernst redox equation:

$$E_{redox} = \frac{RT}{zF} ln \frac{\gamma_{c_H} c_H}{\gamma_{c_L} c_L} \tag{11}$$

$R$, $T$, $z$, $F$, $\gamma$, $c_{H,}$ and $c_L$ are gas constant, temperature, charge number, Faraday constant, mean activity coefficient, high concentration, and low concentration, respectively. Where $R$, $T$, $z$, and $F$ are described above, and activity coefficient $\gamma$ of different solution concentrations are listed on **Table 1**.[58] Three calculated $E_{redox}$ of 5-fold (0.1 M/0.5 M), 50-fold (0.01 M/0.5 M) and 500-fold (0.001 M/0.5 M) NaCl salinity gradient systems are 37.8 mV, 93.4 mV, and 150.9 mV.

Usually, in a salinity gradient system, it assumes a stable interface between the two concentrations and ion exchanging at a reversable state in a very low rate, we should consider a transfer $E_{redox}$, which is a sum of the redox potential above and the osmotic potential.[57] However, in this cylindrical channel model, as its diameter is on sub-micro scale, we consider the high ionic flux across membrane could not be treated as thermodynamic equivalence, and the ion current would not be limited by ionic

**Table 1.** Simulated results of Nernst redox equation in 5-fold, 50-fold, and 500-fold NaCl salinity gradient system, with calculated $E_{redox}$ and corresponding activity coefficient $\gamma$ for comparison.

| Concentration Gradient [M/M] | $E_{Cl-}$ [mV] | $E_{Na+}$ [mV] | $E_{total}$ [mV] | $I_{0,\,Cl-}$ [μA] | $I_{0,\,Na+}$ [μA] | $E_{redox}$ [mV] | $\gamma$ of $c_H$ | $\gamma$ of $c_L$ |
|---|---|---|---|---|---|---|---|---|
| 0.5/0.1 | −40.7 | +40.7 | −8.5 | +4.97 | −3.26 | 37.8 | 0.682 | 0.749 |
| 0.5/0.01 | −98.8 | +98.8 | −20.6 | +6.09 | −3.99 | 93.4 | 0.682 | 0.922 |
| 0.5/0.001 | −157 | +157 | −32.7 | +6.20 | −4.06 | 150.9 | 0.682 | 0.977 |

flux across membrane. Also, for an Ag/AgCl electrode in NaCl solution, the output current occurs due to reduction or oxidation reaction of $Cl^-$ on the interface between electrode and solution. In addition, as the two buffering pools are large enough, ion exchanging and reaction would not affect their bulk concentrations. So, in this power conversion system, we suggest measured ionic current was contributed only by $Cl^-$ ionic flux reacted on Ag/AgCl electrodes, which is smaller than a sum of $Na^+$ and $Cl^-$ fluxes across the membrane, while the $Na^+$ ionic flux was also an important affecting factor to the system. The measured current could be represented by Equation (12):

$$I_{z,\,i} = Fz_i \iint J_{z,\,i} ds,\ i = Cl^- \tag{12}$$

Also, the boundary conditions of external applied voltage and ground potential could represent measured potential on the pair of Ag/AgCl electrodes in experiment.

Firstly, we set this model with condition that the channel surface was neutral charged, *I–V* characteristic curves of the 5-fold, 50-fold, and 500-fold systems were simulated for diffusion without affection from charged channel surface. With the PNP equations assumption, simulated total current is a sum of $Cl^-$ and $Na^+$ ionic fluxes. Simulated results are shown in Figure S1 (Supporting Information). For each *I–V* curve, we could acquire an open-circuit voltage or $V_{OC}$ on the point crossing *x*-axis. From the three curves $Cl^-$, $Na^+$ currents and total current in Figure S1 (Supporting Information) of the 500-fold system as an example, the $V_{OC}$ of $Cl^-$ ionic current curve is −157 mV and of $Na^+$ ionic flux curve is +157 mV. These two voltages could refer the calculated monovalent non-transfer $E_{redox}$ from Nernst equation above, and here recorded as $E_{Cl-}$ and $E_{Na+}$ separately. The $V_{OC}$ of total current is −32.7 mV, refers osmotic potential of total ionic flux in solution without external applied voltage, and recorded as $E_{total}$ here. For transfer $E_{redox}$ of $Cl^-$, we have $E_{total} - E_{Cl-} = 124.3$ mV, and of $Na^+$ is $E_{Na+} - E_{total} = 189.7$ mV. We could also acquire a short-circuit current or $I_{SC}$ from *I–V* curve of $Cl^-$ or $Na^+$ current on the point crossing *y*-axis and recorded as $I_{0,\,Cl-}$, $I_{0,\,Na-}$ separately. For this 500-fold system, $I_{0,\,Cl-}$ is +6.20 μA and $I_{0,\,Na-}$ is −4.97 μA. We could check transfer number of $Cl^-$ and $Na^+$ in NaCl aqua solution by Equations (13) and (14):

$$t_- = \frac{\left|I_{0,Cl^-}\right|}{\left|I_{0,Na^+}\right| + \left|I_{0,Cl^-}\right|} = \left|\frac{E_{Na^+} - E_{total}}{E_{Na^+} - E_{Cl^-}}\right| = 0.604 \tag{13}$$

$$t_+ = \frac{\left|I_{0,Na^+}\right|}{\left|I_{0,Na^+}\right| + \left|I_{0,Cl^-}\right|} = \left|\frac{E_{Cl^-} - E_{total}}{E_{Cl^-} - E_{Na^+}}\right| = 0.396 \tag{14}$$

which fit $t_- = \frac{D_-}{D_+ + D_-}$ and $t_+ = \frac{D_+}{D_+ + D_-}$ with substitution of diffusion coefficients $D$-($Cl^-$) and $D_+$ ($Na^+$) set in model as $2.03 \times 10^{-9}$ $m^2\ s^{-1}$ and $1.33 \times 10^{-9}$ $m^2\ s^{-1}$. Similar transfer number calculating results could also be acquired from the 50-fold and 5-fold systems by their own $E_{Cl-}$, $E_{Na+}$, $E_I$, $I_{0,\,Cl-}$, and $I_{0,\,Na-}$ listed in Table 1. This step demonstrates a way to simulate redox potential directly and simply from PNP equations model, so that we could consider salinity gradient potential in this ion channel system model. The deviation less than 8% from Nernst equation might due to activity coefficient of strong monovalent ion is neglected in this model of dilute aqua solution, as charge continuum is a basic assumption to PNP and PNP-NS equations. Also, transfer number of each ion could be roughly estimated from simulated $V_{OC}$ in Equations (13) and (14).

### 2.2. Experiment for Ion Conductance and Osmotic Energy Conversion Property of the High Ionic Flux Sub-Micro Glass Channels Membrane

To build a high ionic flux salinity gradient power generation system, a glass channels membrane (Figure 2a) was fabricated. This membrane contains a large quantity of symmetric cylindrical channels in a uniform size, ≈900 nm diameter (Figure 2b) and 200 μm length (Figure 2c). It clearly reveals a $6.6 \times 10^7$ $cm^{-2}$ pore-density of membrane, corresponding to a porosity of 42.76%, by counting the top-view SEM image of this membrane in Figure 2b. The geometry of one channel and porosity of membrane was almost the same as we set in the model above. Here, the high pore-density could provide sufficient space for ion transport across membrane in electrolyte solution. X-ray photoelectron spectroscopy (XPS) analysis was used to detect constituent elements of this glass membrane. As shown in Figure S2 (Supporting Information), the XPS spectrum of primary glass channels membrane exhibits O1s, Si1s, and Si2p signals. In aqua solution, Zeta potential of glass drops to zero when pH is near 2.7, so its isoelectric point values (pI) is 2.7, and possesses negative surface charge in neutral pH.[38]

To assemble experiment device, the glass channels membrane was sandwiched in the middle of electrolytic cell, and two concentrations of electrolyte solutions were filled on each side of buffering pools. First, properties of ion across membrane were investigated by measuring *I–V* curves with a series concentration ($10^{-6}$-1 M) of NaCl solution, here in the device both sides of electrolyte buffering pools were filled with same concentrations in sequence, results are shown in **Figure 3**. When concentration decreased below 10 mM to 1 μM, the degree of decline on ionic current is not as much as the degree as concentration dropped from 1 M to 10 mM. Ionic conductance of glass channels

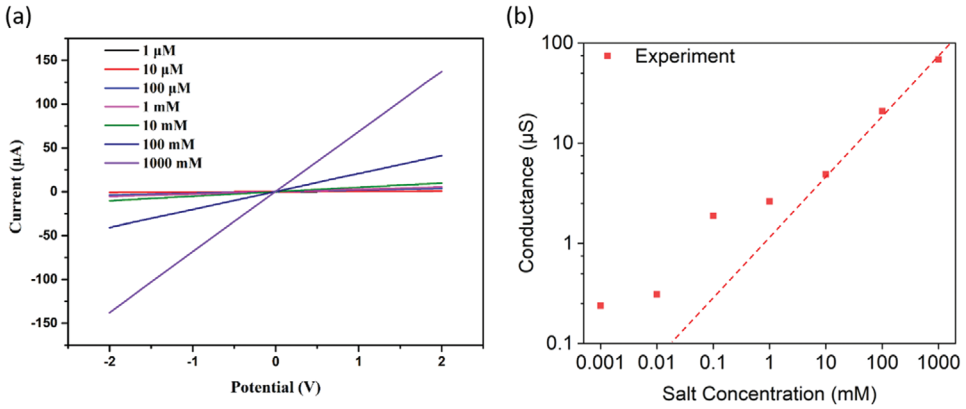


**Figure 3.** a) I–V curves of the glass channels membrane in different electrolyte concentrations (1 μM-1000 mM). b) Ionic conductance of the glass channels membrane as a function of the electrolyte concentration.

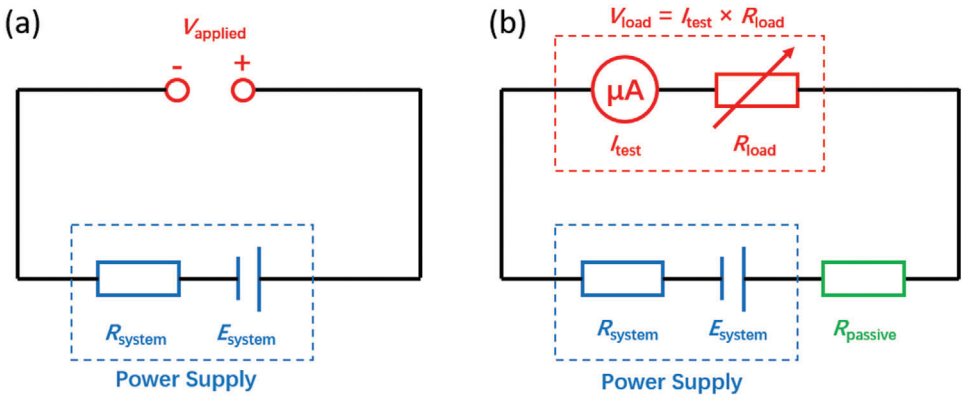


**Figure 4.** Electric circuit diagrams of a) I–V curve characteristic testing device and b) output osmotic power recording device.

membrane deviates from bulk value when concentration is less than 10 mM, shown as red line (linear relationship of ionic conductance with the electrolyte concentration) in Figure 3b. This can be explained by obvious affection of $H^+$ and $OH^-$ at very low bulk concentration.[38]

Then we studied osmotic energy conversion properties of this glass channels membrane in salinity gradient. Electric circuit diagram of I-V characteristic curve testing device is described in **Figure 4**a. Here, to build 500-fold, 50-fold, and 5-fold salinity gradient systems, for each group of experiment, 0.001 M, 0.01 M, and 0.1 M low concentrations of NaCl solutions were filled on left side of buffering pool separately, and 0.5 M high concentration NaCl solutions was filled on the right side, as shown in Figure 1a. External voltage $V_{applied}$ was applied to this experiment device and corresponding output current $I$ was measured, with a tested area $S_{test}$ of $3 \times 10^4$ μm$^2$, so that we could calculate current density $J = I/S_{test}$. In **Figure 5**a, I–V characteristic curve of each system was recorded. As a consequence, $I_{SC}$ and $V_{OC}$ can be directly obtained from the intercept by coordinate axes of each line.[27] Inner resistance of this power generation system, calculated in **Table 2** (defined as $R_{system} = -V_{OC}/I_{SC}$), is ≈21 kΩ under the 500-fold gradient.[35] From other $I$–$V$ curves data in Table 2, inner resistances are calculated ≈14 kΩ under the 0.01 M/0.5 M 50-fold NaCl gradient, and 37 kΩ under the 0.1 M/0.5 M 5-fold NaCl gradient. The much higher inner resistance under 0.1 M/0.5 M 5-fold NaCl gradient indicates ion transport resistance in this low salinity gradient may not mainly exist on ion across channel comparing with 500-fold and 50-fold systems.

To record output osmotic powers, we connected a resistance box as an external electrical load to the three systems of 500-fold, 50-fold, and 5-fold gradients, and adjusted a series of resistances. Here the power supply is osmotic power generation system tested above. The curves of output power density and current density of glass channels membrane to various salinity gradient systems as a function of external resistance are shown in Figure 5b–d. We can see the highest output power densities are 4.16 W m$^{-2}$ (at 7 kΩ) and 0.40 W m$^{-2}$ (at 20 kΩ) for the 50-fold (Figure 5c), 5-fold (Figure 5d) systems, respectively. In particular, value of the highest power density is up to 7.91 W m$^{-2}$ (at 10 kΩ) when the salinity gradient was 500-fold (Figure 5b).

To furthering discuss relationship between $I$-$V$ curve characteristics and output osmotic power properties of the 0.001 M/0.5 M 500-fold NaCl gradient system, first we can notice for the almost straight slope $I$–$V$ curve of this system in Figure 5a, its theoretical highest power output state would be situated at a

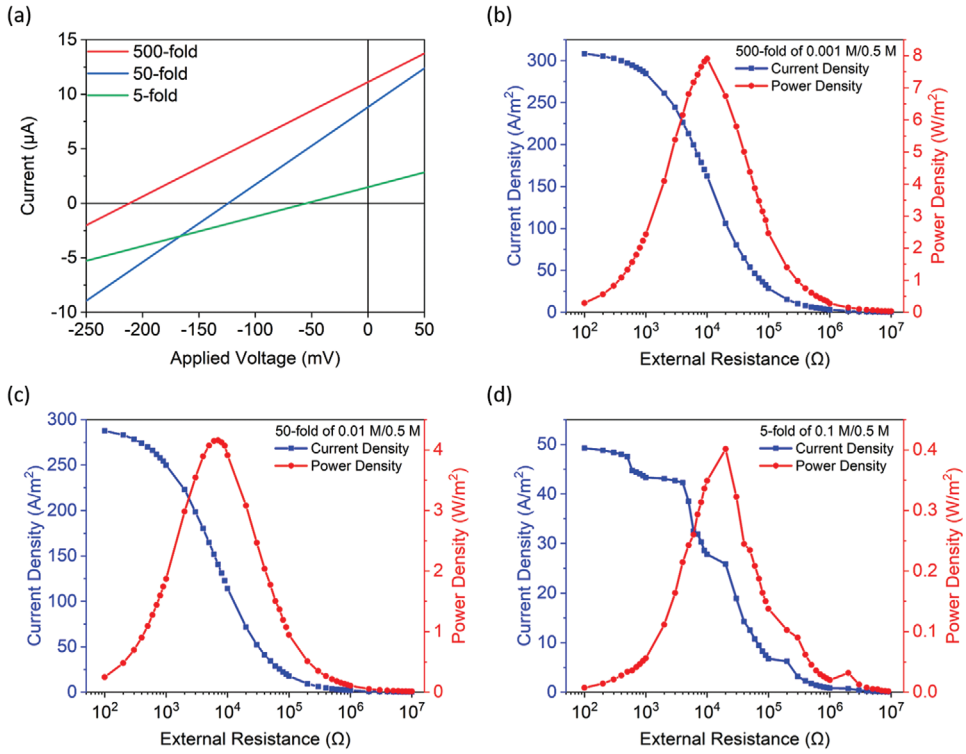


**Figure 5.** Osmotic energy conversion property of the glass channels membrane. a) *I-V* curves under the 500-fold (red), 50-fold (blue), and 5-fold (green) salinity gradient systems of the glass channels membrane. Output current densities and power densities of the glass channels membrane with external electrical load obtained at b) 500-fold, c) 50-fold, and d) 5-fold concentration gradients. The peak values of output power densities are 7.91 W $m^{-2}$, 4.16 W $m^{-2}$, and 0.40 W $m^{-2}$ separately.

**Table 2.** The corresponding $I_{SC}$, $J_{SC}$, $V_{OC}$, $R_{system}$, $J_{Pmax,I\text{-}V}$, $V_{Pmax,I\text{-}V}$ of *I-V* characteristic curves and $P_{max}$, $R_{load}$, $J_{Pmax,load}$, $V_{Pmax,load}$ of external electrical load curves in experiments.

| Concentration Gradient [M/M] | $I_{SC}$ [μA] | $J_{SC}$ [A $m^{-2}$] | $-V_{OC}$ [mV] | $R_{system}$ [kΩ] | $J_{Pmax,I\text{-}V}$ [A $m^{-2}$] | $V_{Pmax,I\text{-}V}$ [mV] | $P_{max}$ [W $m^{-2}$] | $R_{load}$ [kΩ] | $J_{Pmax,load}$ [A $m^{-2}$] | $V_{Pmax,load}$ [mV] |
|---|---|---|---|---|---|---|---|---|---|---|
| 0.5/0.1 | 1.48 | 49.3 | 54.8 | 37 | 24.6 | 27.4 | 0.40 | 20 | 25.8 | 15.5 |
| 0.5/0.01 | 8.82 | 294 | 124.1 | 14 | 147 | 62.1 | 4.16 | 7 | 138 | 29.6 |
| 0.5/0.001 | 10.07 | 336 | 211.7 | 21 | 168 | 106 | 7.91 | 10 | 162 | 48.7 |

theoretically current density $J_{Pmax,I\text{-}V}$ and its corresponding output voltage $V_{Pmax,I\text{-}V}$ from I–V curve data in Table 2 by Equations (15) and (16):

$$J_{Pmax,I-V} = 1/2 J_{SC} = 168\ \text{A m}^{-2} \quad (15)$$

$$V_{Pmax,I-V} = -1/2 V_{OC} = 106\ \text{mV} = 0.106\ \text{V} \quad (16)$$

Considering this system in a circuit with only resistance loads, while the power supply outputting its maximum power, for the system all external resistance in circuit is equal to internal resistance of power supply, so that in this system we have Equation (17):

$$R_{circuit} = R_{system} = 21\ \text{k}\Omega \quad (17)$$

where $R_{system}$ has been defined above, here could be described as internal resistance of the salinity gradient system power supply, and $R_{circuit}$ means all the other resistance in the circuit.[43]

From the external electrical load curve in Figure 5b and corresponding data in Table 2, we can see while $R_{load}$ = 10 kΩ, with corresponding tested current density $J_{Pmax,load} = I_{Pmax,load}/S_{test}$ = 162 A $m^{-2}$, the measured output power density reached its peak value $P_{max}$ calculated by Equation (18):

$$P_{max} = I^2_{Pmax,load} \times R_{load}/S_{test} = V_{Pmax,load} \times J_{Pmax,load} = 7.91\ \text{W m}^{-2} \quad (18)$$

Here, the voltage $V_{Pmax,load}$ over resistance box can be calculated by Equation (19):

$$V_{P\,max,load} = P_{max}/J_{Pmax,load} = 48.7\ \text{mV} = 0.0487\ \text{V} \quad (19)$$

Comparing current densities of the theoretical highest power output state from *I–V* curve and the tested highest output power density from external electrical load curve, we have $J_{Pmax,I\text{-}V} \approx J_{Pmax,load}$, so we could confirm this 500-fold gradient system working at the theoretically state above, with a corresponding output potential $V_{Pmax,I\text{-}V} = 0.106$ V. But as $R_{load} < R_{channel}$, we may consider a resistance $R_{passive}$ caused by passive ion transportation obstruction without a forced external applied voltage over the two buffering pools on *I–V* curves test, so we have Equation (20) at the highest power output state with external electrical load:

$$R_{circuit} = R_{load} + R_{passive} = 21\,k\Omega \tag{20}$$

while $R_{load} = 10$ kΩ. The whole electric circuit diagram of this output osmotic power recording device could be described in Figure 4b. In our reported work about salinity gradient system with the same experiment device, this relationship between *I–V* curve and external electrical load curve is also existed.[54]

For the 0.01 M/0.5 M 50-fold system, with the same method from Equation (15) to (20), at the theoretical highest power output calculated from Table 2, we can also obtain $R_{circuit} = 14$ kΩ, and theoretically current $J_{Pmax,I\text{-}V} = 147$ A m$^{-2}$, corresponding output voltage $V_{Pmax,I\text{-}V} = 0.0621$ V. From the external electrical load curve in Figure 5c, at the measured highest 4.16 W m$^{-2}$ output power density, we have $J_{Pmax,load} = 138$ A m$^{-2}$, $V_{Pmax,load} = 0.0296$ V, when $R_{load} = 7$ kΩ. Also, in this 50-fold gradient system, we have $J_{Pmax,load} \approx J_{Pmax,I\text{-}V}$, with a corresponding output potential $V_{Pmax,I\text{-}V} = 0.0621$ V.

For the 0.1 M/0.5 M 5-fold system, also with Equation (15) to (20), at the theoretical highest power output calculated from Table 1, we have $R_{circuit} = 37$ kΩ, theoretically current $J_{Pmax,I\text{-}V} = 24.6$ A m$^{-2}$, corresponding output voltage $V_{Pmax,I\text{-}V} = 0.0274$ V. From the external electrical load curve in Figure 5d, at the measured highest 0.40 W m$^{-2}$ output power density, $J_{Pmax,load} = 25.8$ A m$^{-2}$, $V_{Pmax,load} = 0.0155$ V, when $R_{load} = 20$ kΩ. Here, $J_{Pmax,load} \approx J_{Pmax,I\text{-}V}$ is also existed, with a corresponding output potential $V_{Pmax,I\text{-}V} = 0.0274$ V. However, in Figure 5d, we can see the two curves of output current density and output power density are not smooth, this also indicates ion transportation has high interference in this low concentration gradient system, and leads to a high electrical resistance in the circuit.

**Table 3.** Model parameters for ionic conductance simulation of the glass channels membrane.

| Concentration [M] | 0.001 | 0.01 | 0.1 | 1 |
|---|---|---|---|---|
| Surface charge density [C m$^{-2}$] | −0.005 | −0.010 | −0.015 | −0.020 |
| $\zeta_s$ on channel wall [mV] | +90 | +0 | −60 | −90 |

## 2.3. PNP-NS Numerical Simulation and Mechanism Study of the Model of High Ionic Flux Sub-Micro Channel

### *2.3.1. Ion Conductance Simulation of High Ionic Flux Sub-Micro Channel*

For different structure of ion channel, the interaction between surface charge on channel wall and ion solution could be quite different, but this property could be described by ion conductance of system overall.[38] Here, ion conductance simulation was performed to verify our PNP-NS equations model of the high ionic flux sub-micro channel. As mentioned above, to simulate ion transportation by PNP-NS equations, surface charge density $\sigma_s$ of glass channel and $\zeta_s$ on glass channel wall are needed.

Surface charge density of $SiO_2$ glass channel is on −0.01 C m$^{-2}$ magnitude in 1 mM to 1 M NaCl aqua solution with pH 7.[39,52] Also it can be derivated from $\zeta$ or zeta potential of the shear plane in solution. However, in continuum model without special consideration of ion charge size in solution, $\zeta_s$ on glass channel wall for electroosmosis described by NS equations is chosen for ion conductance simulation.[51,53,55] The conditions on **Table 3** were used for ion conductance I–V curve simulation of electrolyte concentration from 1 mM to 1 M. As this simulation was performed in COMSOL software, the mesh building for finite element method numerical simulation is described in SI, grid independence verification result is also listed in Table S1 (Supporting Information).[59,60]

**Figure 6** could verify surface charge density conditions set in the four models. Figure 6a is $Na^+$ normalized concentration distribution at the middle section of channel at 0 V applied voltage. It shows for all the four sub-micro channel system, $Na^+$ concentrations decrease from channel wall in 5 to 40 nm, this distance could represent diffuse layer of electric double layer (EDL) in continuum model.[56] $Na^+$ concentrations would approach their bulk

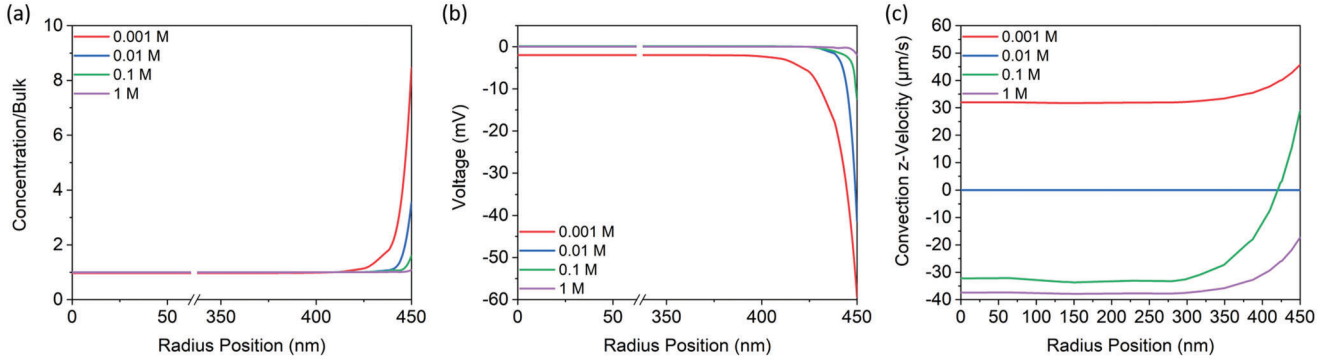


**Figure 6.** a) $Na^+$ concentration distribution and b) potential distribution at the middle section of channel at 0 V applied voltage. c) Convection velocity in *z*-direction (or along the axis) at −0.1 V applied voltage. Bulk concentration of 0.001 M (red), 0.01 M (blue), 0.1 M (green), and 1 M (purple) were simulated.

**Table 4.** Simulated results for ionic conductance of the glass channels membrane. Calculated $\zeta$ potential and experiment conductance for comparison.

| Concentration [M] | 0.001 | 0.01 | 0.1 | 1 |
|---|---|---|---|---|
| $\zeta = -20 \cdot p[Na+]$ [mV] | −60 | −40 | −20 | 0 |
| $\zeta$ [mV] ~ [Na+]−1/2 | – | – | −12.6 | −4 |
| PNP-NS $\zeta$ potential [mV] | −57.4 | −41.4 | −12.6 | −1.96 |
| Exp. Conductance [μS] | 2.63 | 4.89 | 20.9 | 68.7 |
| PNP-NS Conductance [μS] | 0.86 | 4.90 | 20.7 | 70.1 |
| PNP Conductance [μS] | 0.49 | 4.90 | 49.6 | 497 |

values on the axis of channel defined as 0 nm. So, the $\zeta$ potential for each concentration system could refer to $Na^+$ concentration along the axis of channel in vertical direction.

For pH 7 NaCl solution on $SiO_2$ glass, we have $\zeta = -20$ mV • p[$Na^+$], where [$Na^+$] is the bulk value of concentration in mol $L^{-1}$. Particularly, for $|\zeta|$ below 40 mV, $\zeta \sim [Na^+]^{-1/2}$ is also a well derivation.[38] Calculated $\zeta$ potentials by theory were listed on **Table 4**. Figure 6b is potential distribution of solution space at the middle section of channel at 0 V applied voltage. Figure 6c is convection velocity in *z*-direction (or along the axis) at −0.1 V applied voltage, we can see streaming flows steady near the axis of channel, and convection is also existed at the 450 nm boundary of ion space, which contacting to channel wall boundary. As PNP-NS equations continuum charge assumption is without special consideration of ion charge size in solution, solution space at 450 nm is the nearest to shear plane, so we would calculate simulated $\zeta$ potential by the potential difference of solution space between 450 nm and 0 nm. Simulated $\zeta$ potential result on Table 4 matches the theory result, as −57.4 mV, −41.4 mV, −12.6 mV, −1.96 mV of the 0.001 M, 0.01 M, 0.1 M, and 1 M models, it shows our estimation of surface charge density is reliable.

**Figure 7** is simulation results of I–V curves and corresponding ionic conductance, results of 0.01 M, 0.1 M, and 1 M could accurately match experimental results, and keeps linear to 0.001 M. While in realistic solution of 1 mM bulk concentration or lower, $H^+/OH^-$ balance cannot be neglect, but it was not considered in this model and result in the deviation. Simulated ionic conductance compared with experiment is listed in Table 4.

As ion charge size is without special consideration in PNP-NS equations model, the potential $\zeta_s$ on glass channel wall was set to fit ion conductance experiment, with affection from sub-micro channel structure in consideration, and the $\zeta$ potential in shear plane of solution was checked by simulated result. While the structure of EDL between the two planes was not especially considered. However, we could demonstrate it qualitatively. Surface charge densities of the 0.001 M, 0.01 M, 0.1 M, and 1 M models are −0.005 C $m^{-2}$, −0.01 C $m^{-2}$, −0.015 C $m^{-2}$, and −0.02 C $m^{-2}$ in model, with higher negative charge density on glass channel wall, its $\zeta_s$ potential could be lower.

Also, PNP model results with the same surface charge density were simulated and compared in Table 4. It deviates experiment, which indicates PNP model is not suit in this sub-micro channel with electroosmosis in consideration.

With the comparison among experiment, PNP equations model and PNP-NS equations model, we can see in the 0.001 M model, ion convection flux is positive to ion conductance, while in the 0.1 M model and 1 M model ion convection flux is negative to ion conductance.

According to this ion conductance simulation, the PNP-NS model with its boundary conditions, and the assumption that ionic currents are contributed by $Cl^-$ ionic flux across the membrane, could be used to further mechanism study for salinity gradient system with this high ionic flux membrane in the range from 0.01 to 1 M concentration, and extrapolate to 0.001 M partly.

### *2.3.2. I–V Curves Simulation of Salinity Gradient System with Charged High Ionic Flux Membrane*

To simulate *I–V* characteristic curves of the 500-fold, 50-fold, and 5-fold gradient systems within the range for power outputting, it was performed under applied voltage from −250 mV to +50 mV. A 10 μm length channel model was used for facilitation in salinity gradient system simulation with less calculation. This shortened channel has 20 times lower current resistance than the original 200 μm length channel, and we adjusted simulated currents with this factor. Ion conductance of the two channel models is

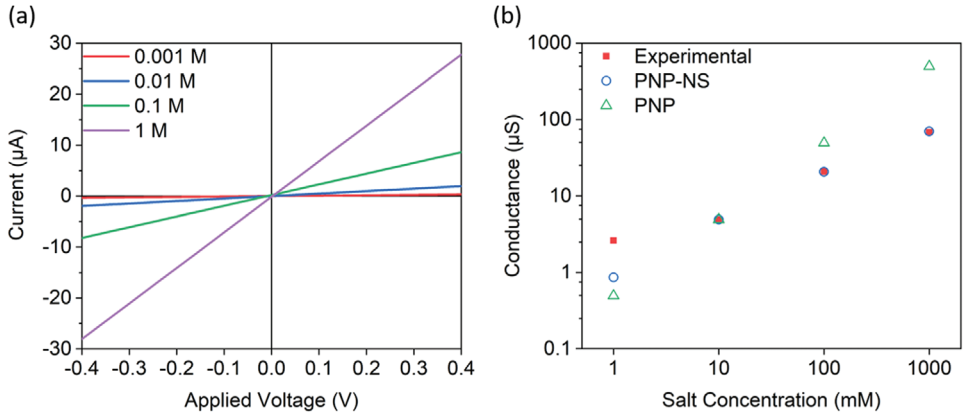


**Figure 7.** a) I–V curves simulation of the glass channel in different electrolyte bulk concentrations as 0.001 M (red), 0.01 M (blue), 0.1 M (green), and 1 M (purple). b) Ionic conductance simulation results of the glass channel as a function of the electrolyte bulk concentration. The PNP-NS simulation (blue circle) was compared to experiment results (red square) and PNP simulation (green triangle).

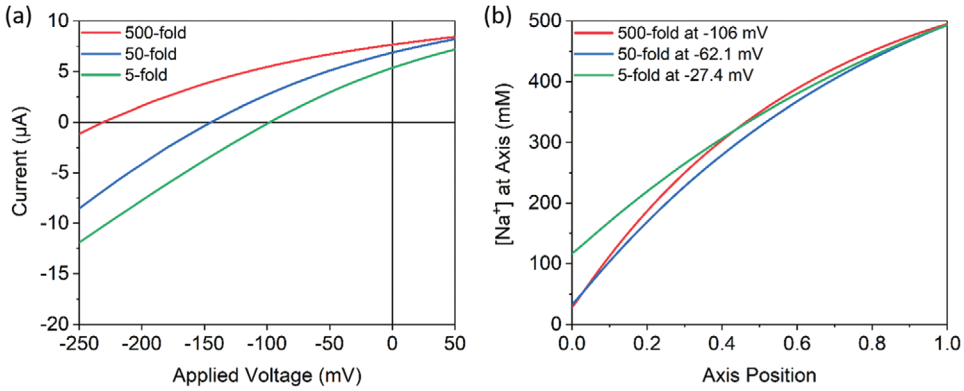


**Figure 8.** a) Simulation for I-V curves of 500-fold (red), 50-fold (blue), and 5-fold (green) gradient systems. b) $Na^+$ concentration distribution along the axis of 500-fold (red), 50-fold (blue), and 5-fold (green) gradient systems at their own $-V_{Pmax,I\text{-}V}$ of 106 mV, 62.1 mV, and 27.4 mV.

**Table 5.** Simulated data $I_{SC,Sim}$, $V_{OC,Sim}$, $J_{Pmax,Sim}$, $V_{OC,Na+}$, $V_{OC,total}$, and $t_{+,sim}$ of the 5-fold, 50-fold and 500-fold salinity gradient system models. $I_{SC}$, $V_{OC}$, $J_{Pmax,I\text{-}V}$, $V_{Pmax,I\text{-}V}$ in experiment of each system for comparison.

| Concentration Gradient [M/M] | $I_{SC}$ [μA] | $V_{OC}$ [mV] | $J_{Pmax,I\text{-}V}$ [A $m^{-2}$] | $V_{Pmax,I\text{-}V}$ [mV] | $I_{SC,Sim}$ [μA] | $V_{OC,Sim}$ [mV] | $J_{Pmax,Sim}$ [A $m^{-2}$] | $V_{OC,Na+}$ [mV] | $V_{OC,total}$ [mV] | $t_{+,sim}$ |
|---|---|---|---|---|---|---|---|---|---|---|
| 0.5/0.1 | 1.48 | −54.8 | 24.6 | 27.4 | 5.36 | −97.8 | 133 | +25.9 | −8.8 | 0.719 |
| 0.5/0.01 | 8.82 | −124.1 | 147 | 62.1 | 6.88 | −144.6 | 148 | +82.3 | −21.2 | 0.544 |
| 0.5/0.001 | 10.07 | −211.7 | 168 | 106 | 7.65 | −230.8 | 171 | +145.4 | −33.9 | 0.523 |

compared in Table S1 (Supporting Information), the shortened channel could be used to discuss solution in 0.001 M to 0.5 M.

As discussed above, simulated $Cl^-$ ionic flux and corresponding applied voltage would be chosen to represent measured output current. The I-V curves are shown in **Figure 8**a, and characteristic data $I_{SC,Sim}$, $V_{OC,Sim}$ are shown in **Table 5**. For simulation results of the 500-fold model, we can see a $V_{OC,Sim}$ of −230.8 mV and a $I_{SC,Sim}$ of 7.65 μA. For the 50-fold model, here are a $V_{OC,Sim}$ of −144.6 mV and a $I_{SC,Sim}$ of 6.88 μA. And for the 5-fold model are a $V_{OC,Sim}$ of −97.8 mV and a $I_{SC,Sim}$ of 5.36 μA.

In this model, we assumed inner resistance of power generation system is concentrated on ion channel, which would be smaller than actual inner resistance in experiment device. Ion across channel resistance is dominant in 50-fold and 500-fold systems, so the simulated $V_{OC,Sim}$ −144.6 mV and −230.8 mV are slightly higher than the $V_{OC}$ −124.1 mV and −211.7 mV tested in experiment. On the other hand, these PNP-NS equations simulations were performed at steady-state, while the *I–V* curves in experiment were scanned, the simulated $I_{SC,Sim}$ would be smaller than corresponding tested $I_{SC}$. As discussed above, inner resistance of the 5-fold low gradient system is not mainly existed on ion across channel, so the simulated $I_{SC,Sim}$ and $V_{OC,Sim}$ would be higher, however it obeys the trend in experiment comparing with the 50-fold and 500-fold systems.

If we inspect simulated I-V curves at $V_{Pmax,I\text{-}V}$, as 106 mV, 62.1 mV, 27.4 mV of 500-fold, 50-fold, 5-fold systems tested in experiment, the corresponding simulated current density $J_{Pmax,Sim}$ are 171 A $m^{-2}$, 148 A $m^{-2}$, 133 A $m^{-2}$. The 500-fold and 50-fold models with high osmotic power output fit experiment well, which could account for the working states while the 500-fold system outputting 7.91 W $m^{-2}$ and the 500-fold system outputting 4.16 W $m^{-2}$.

Figure 8b is $Na^+$ distribution along the axis at $V_{Pmax,I\text{-}V}$. We could notice for the 0.001 M/0.5 M 500-fold system, $Na^+$ concentration reaches higher than 0.01 M while entering ion channel from the left buffering pool, so the deviation of simulated ion conductance at 0.001 M would have limited affection to salinity gradient simulation.

If we estimate cation transfer numbers from simulated $V_{OC}$ of $Cl^-$, $Na^+$ currents and total current as $V_{OC,Sim}$, $V_{OC,Na+}$ and $V_{OC,total}$ in Table 1 following the method $t_+ = |\frac{E_{Cl^-} - E_{total}}{E_{Cl^-} - E_{Na^+}}|$ above, $t_{+,sim}$ of the 500-fold, 50-fold and 5-fold models are 0.523, 0.544, and 0.719, higher than 0.396 in bulk NaCl aqua solution. The result demonstrates this sub-micro negative charged cylindrical channel could also be beneficial to cation transfer through not reach a very high selectivity, especially in the 500-fold and 50-fold models.

Considering ion conductance simulation of 0.01 M 0.1 M, and 1 M models fit experiment well. And comparing simulation and experiment results above, we choose 50-fold gradient system to further study mechanism of ionic flux from simulation result. According to the definition of Nernst-Planck equation, ionic flux is composed of diffusion, electrophoresis and convection. To investigate each contribution of output $Cl^-$ ionic flux current on **Figure 9**a, electrophoresis is proportional to applied voltage in general, while diffusion and convection are positive to ionic current in the working range from *Voc* to 0 V, which indicates both of them facilitate the generation of ionic current and are benefit to energy output. Here, diffusion could keep stable as it is mainly due to concentration gradient, while convection described by electroosmosis is related to voltage. Figure 9b shows solution convection velocity along the axis in *z*-direction under −62.1 mV at 1/4, 1/2, and 3/4 sections of channel. And the direction of solution convection is from high concentration

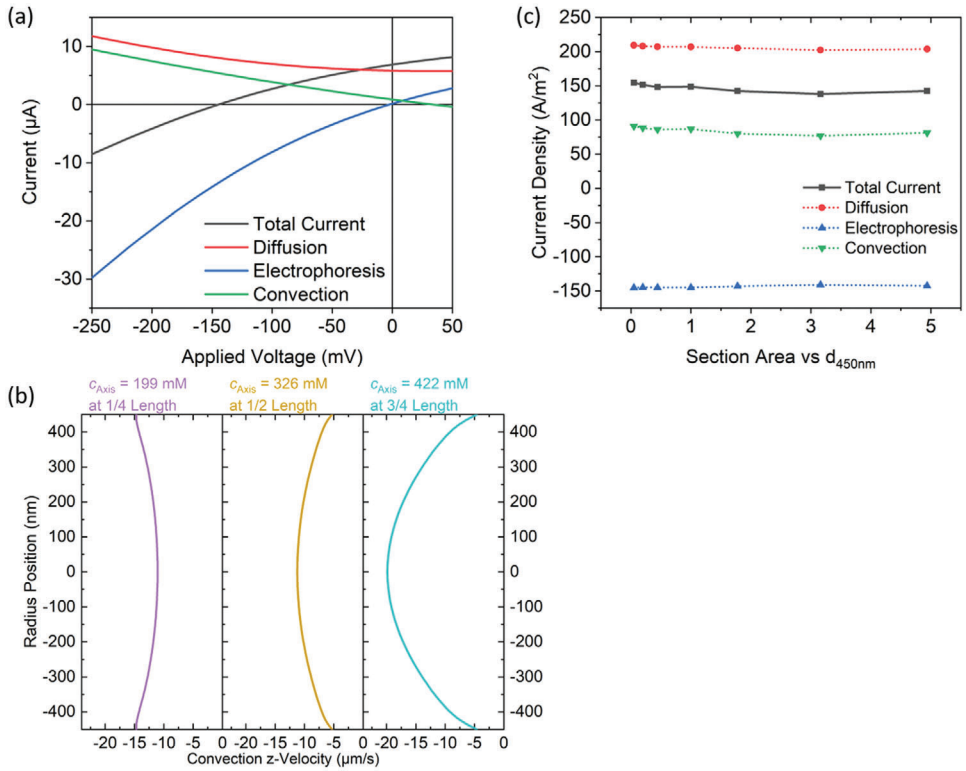


**Figure 9.** a) $Cl^-$ ionic flux current (black) of the 50-fold gradient system varies with external applied voltage, and its composition of diffusion (red), electromigration (blue) and convection (green) fluxes. b) Solution convection velocity along the axis in z-direction under −62.1 mV at 1/4 (purple), 1/2 (yellow), and 3/4 (cyan) sections of channel. c) $Cl^-$ ionic fluxes (black line) of the 50-fold gradient systems in cylindrical channels with different diameters under −62.1 mV applied voltage, and each composition of diffusion (red line), electrophoresis (blue line), convection (green line) fluxes. Channels are listed by ratios of section area.

to low concentration due to electroosmosis initiated by external applied voltage along channel and the negative charged channel surface. Differs from convection in *z*-direction on Figure 6c of ion conductance simulation, solution streaming here flows in a conical velocity distribution.

To study how the three kinds of composition contribute to total flux in sub-micro channel more furtherly, we set cylindrical channel models with 100 nm, 200 nm, 300 nm, 600 nm, 800 nm, and 1000 nm radii, and simulated at −62.1 mV applied voltage, results are shown on Figure 7c. We could see they have consistent properties generally in the 100 to 1000 nm sub-micro range. However, we simply applied the potential $\zeta_s$ on glass channel wall from 450 nm model, ion conductance would actually be tested in further experiment.

## 3. Conclusion

In conclusion, we introduced a numerical simulation model based on numerical simulation model of ion channel with PNP-NS equations with several complements to the assumption for salinity gradient power generation system with a high ionic flux ion channel. In experiment, we applied a high ionic flux glass nanochannels membrane to salinity gradient power generation. In the energy conversion system, the maximum output power of the system can reach a value of 7.91 W $m^{-2}$ under the 500-fold salinity gradient, besides, this value can achieve 4.16 W $m^{-2}$ in the artificial seawater (0.5 M NaCl) and river water (0.01 M NaCl). Numerical simulation to ion conductance experiment indicates our model is reliable for this system. Combining experiment results with simulation, we discussed the glass membrane achieved selectivity of cations while maintaining high ionic throughput, which can improve the output power density of osmotic power generation. In summary, the sub-micro glass channels membrane model showed a good promise for the application of the energy conversion, offering a new view for osmotic energy conversion.

## 4. Experimental Section

*Numerical Simulation*: The mechanism of ion transport and ion concentration inside the channels were analyzed by using commercial finite-element software package COMSOL Multiphysics on computer. Attempt to simplify the task of theoretical simulation building, the modeling was performed for one cylindrical channel. The details about this simulation model and relevant boundary conditions were shown in the Figure S4 (Supporting Information).

*Electrical Measurements*: The electrical measurements were investigated by a Keithley 6487 picoammeter (Keithley Instruments, Cleveland, OH) with a pair of Ag/AgCl (1 M KCl) electrodes. The glass channels membrane, tested area was $3 \times 10^4$ $\mu m^2$, was sandwiched between two parts of the electrolytic cell in measurement. Two sides of the membrane were filled with the symmetric concentration electrolyte solutions (NaCl) from 1 μM to 1 M for test ionic transport properties. In energy conversion

properties measurements, two sides were filled with different concentration electrolyte solutions forming salinity gradient ($c_H/c_L$ = 5-fold, 50-fold, 500-fold). The solutions used in the experiment were prepared with Milli-Q water (18.2 MΩ).

The ionic transport properties and energy conversion properties were investigated by measuring ionic current. Ionic current was measured by a Keithley 6487 picoammeter (Keithley Instruments, Cleveland, OH) with a pair of Ag/AgCl electrodes. The I–V curves were tested with scanning voltage swept from −2 to +2 V at a scan rate of 0.2 V $s^{-1}$. The glass channels membrane was sandwiched between two parts of the electrolytic cell in experimentally measurement.

## Supporting Information

Supporting Information is available from the Wiley Online Library or from the author.

## Acknowledgements

This work was supported by the National Key Research and Development Program of China (2022YFB3805901, 2022YFB3805900), the National Natural Science Foundation of China (21975009), and Beijing Natural Science Foundation (2202025).

## Conflict of Interest

The authors declare no conflict of interest.

## Data Availability Statement

The data that support the findings of this study are available from the corresponding author upon reasonable request.

## Keywords

high ionic flux, PNP-NS equations model, salinity gradient power generation, sub-micro glass channels membranes

Received: May 8, 2023
Revised: July 14, 2023
Published online: August 13, 2023

[1] S. Chu, A. Majumdar, *Nature* **2012**, *488*, 294.
[2] K. Kowalski, S. Stagl, R. Madlener, I. Omann, *Eur. J. Oper. Res.* **2009**, *197*, 1063.
[3] A. M. Omer, *Renew. Sust. Energ. Rev.* **2008**, *12*, 2265.
[4] J. Gao, W. Guo, D. Feng, H. Wang, D. Zhao, L. Jiang, *J. Am. Chem. Soc.* **2014**, *136*, 12265.
[5] B. E. Logan, M. Elimelech, *Nature* **2012**, *488*, 313.
[6] N. Y. Yip, A. Tiraferri, W. A. Phillip, J. D. Schiffman, L. A. Hoover, Y. C. Kim, M. Elimelech, *Environ. Sci. Technol.* **2011**, *45*, 4360.
[7] P. Długołęcki, K. Nymeijer, S. Metz, M. Wessling, *J. Membr. Sci.* **2008**, *319*, 214.
[8] J. W. Post, J. Veerman, H. V. Hamelers, G. J. Euverink, S. J. Metz, K. Nymeijer, C. J. Buisman, *J. Membr. Sci.* **2007**, *288*, 218.
[9] T. Thorsen, T. Holt, *J. Membr. Sci.* **2009**, *335*, 103.
[10] A. Achilli, T. Y. Cath, A. E. Childress, *J. Membr. Sci.* **2009**, *343*, 42.
[11] K. Lee, R. Baker, H. Lonsdale, *J. Membr. Sci.* **1981**, *8*, 141.
[12] D. A. Vermaas, M. Saakes, K. Nijmeijer, *J. Membr. Sci.* **2011**, *385*, 234.
[13] J. W. Post, H. V. Hamelers, C. J. Buisman, *Environ. Sci. Technol.* **2008**, *42*, 5785.
[14] E. B. Kalman, I. Vlassiouk, Z. S. Siwy, *Adv. Mater.* **2008**, *20*, 293.
[15] D. A. Vermaas, M. Saakes, K. Nijmeijer, *Environ. Sci. Technol.* **2011**, *45*, 7089.
[16] A. L. Myers, J. M. Prausnitz, *AIChE J* **1965**, *11*, 121.
[17] Z. Jia, B. Wang, S. Song, Y. Fan, *Renew. Sust. Energ. Rev.* **2014**, *31*, 91.
[18] Y. Zhu, K. Zhan, X. Hou, *ACS Nano* **2018**, *12*, 908.
[19] R. Li, X. Fan, Z. Liu, J. Zhai, *Adv. Mater.* **2017**, *29*, 1702983.
[20] X. Hou, *Adv. Mater.* **2016**, *28*, 7049.
[21] W. Guo, Y. Tian, L. Jiang, *Acc. Chem. Res.* **2013**, *46*, 2834.
[22] T. Xiao, Q. Zhang, J. Jiang, J. Ma, Q. Liu, B. Lu, Z. Liu, J. Zhai, *Energy Technol.* **2019**, *7*, 1800952.
[23] G. Z. Ramon, B. J. Feinberg, E. M. Hoek, *Energy Environ. Sci.* **2011**, *4*, 4423.
[24] J. Veerman, R. De Jong, M. Saakes, S. Metz, G. Harmsen, *J. Membr. Sci.* **2009**, *343*, 7.
[25] J. Kim, S. J. Kim, D.-K. Kim, *Energy* **2013**, *51*, 413.
[26] F. Yan, L. Yao, K. Chen, Q. Yang, B. Su, *J. Mater. Chem. A* **2019**, *7*, 2385.
[27] D.-K. Kim, C. Duan, Y.-F. Chen, A. Majumdar, *Microfluid Nanofluidics* **2010**, *9*, 1215.
[28] J. Ji, Q. Kang, Y. Zhou, Y. Feng, X. Chen, J. Yuan, W. Guo, Y. Wei, L. Jiang, *Adv. Funct. Mater.* **2017**, *27*, 1603623.
[29] K. Xiao, P. Giusto, L. Wen, L. Jiang, M. Antonietti, *Angew. Chem. Int. Ed. Engl.* **2018**, *57*, 10123.
[30] K. Xiao, L. Chen, R. Chen, T. Heil, S. D. C. Lemus, F. Fan, L. Wen, L. Jiang, M. Antonietti, *Nat. Commun.* **2019**, *10*, 74.
[31] X. Sui, Z. Zhang, C. Li, L. Gao, Y. Zhao, L. Yang, L. Wen, L. Jiang, *ACS Appl. Mater. Interfaces* **2019**, *11*, 23815.
[32] Z. Zhang, X. Sui, P. Li, G. Xie, X. Y. Kong, K. Xiao, L. Gao, L. Wen, L. Jiang, *J. Am. Chem. Soc.* **2017**, *139*, 8905.
[33] X. Huang, Z. Zhang, X.-Y. Kong, Y. Sun, C. Zhu, P. Liu, J. Pang, L. Jiang, L. Wen, *Nano Energy* **2019**, *59*, 354.
[34] Yu, C., Zhu, X., Wang, C., Zhou, Y., Jia, X., Jiang, L., Liu, X., Wallace, G. G., *Nano Energy* **2018**, *53*, 475.
[35] R. Li, J. Jiang, Q. Liu, Z. Xie, J. Zhai, *Nano Energy* **2018**, *53*, 643.
[36] L. Fu, J. Jiang, B. Lu, Y. Xu, J. Zhai, *ChemNanoMat* **2019**, *5*, 1182.
[37] Y. Xu, B. Lu, L. Fu, J. Zhai, *Electrochim. Acta* **2019**, *316*, 266.
[38] B. J. Kirby, E. F. Hasselbrink, Jr, *Electrophoresis* **2004**, *25*, 187.
[39] D. Stein, M. Kruithof, C. Dekker, *Phys. Rev. Lett.* **2004**, *93*, 035901.
[40] S. Brankovic, J. Wang, R. Adžić, *Surf. Sci.* **2001**, *474*, L173.
[41] D.-H. Lin, C.-Y. Lin, S. Tseng, J.-P. Hsu, *Nanoscale* **2015**, *7*, 14023.
[42] V.-P. Mai, R.-J. Yang, *Appl. Energy* **2020**, *274*, 115294.
[43] B. D. Kang, H. J. Kim, M. G. Lee, D.-K. Kim, *Energy* **2015**, *86*, 525.
[44] R. Li, J. Jiang, Q. Liu, Z. Xie, J. Zhai, *Nano Energy* **2018**, *53*, 643.
[45] L. Fu, Y. Wang, J. Jiang, B. Lu, J. Zhai, *ACS Appl. Mater. Interfaces* **2021**, *13*, 35197.
[46] Y. Wang, H. Chen, J. Zhai, *ACS Appl. Mater. Interfaces* **2021**, *13*, 41159.
[47] T.-C. Tsai, C.-W. Liu, R.-J. Yang, *Micromachines* **2016**, *7*, 205.
[48] H. Tao, G. Li, Z. Xu, C. Lian, H. Liu, *Chem. Eng. J.* **2022**, *444*, 136675.
[49] H. Tao, C. Lian, H. Jiang, C. Li, H. Liu, R. van Roij, *AIChE J.* **2022**, *68*, e17549.
[50] H. Tao, C. Lian, H. Liu, *Green Energy Environ.* **2020**, *5*, 303.
[51] S. K. Griffiths, R. H. Nilson, *Anal. Chem.* **1999**, *71*, 5522.
[52] H. Horiuchi, A. Nikolov, D. T. Wasan, *J. Colloid Interface Sci.* **2012**, *385*, 218.
[53] S. K. Griffiths, R. H. Nilson, *Anal. Chem.* **2000**, *72*, 4767.
[54] T. Xiao, B. Lu, Z. Liu, Q. Zhang, J. Zhai, X. Diao, *J. Membr. Sci.* **2022**, *642*, 119999.
[55] R.-J. Yang, L.-M. Fu, C.-C. Hwang, *J. Colloid Interface Sci.* **2001**, *244*, 173.

[56] G. Pardon, W. van der Wijngaart, *Adv. Colloid Interface Sci.* **2013**, *199*, 78.
[57] J. Feng, M. Graf, K. Liu, D. Ovchinnikov, D. Dumcenco, M. Heiranian, V. Nandigana, N. R. Aluru, A. Kis, A. Radenovic, *Nature* **2016**, *536*, 197.
[58] G. N. Lewis, M. Randall, *J. Am. Chem. Soc.* **1921**, *43*, 1112.
[59] R. Long, Z. Kuang, Z. Liu, W. Liu, *Phys. Chem. Chem. Phys.* **2018**, *20*, 7295.
[60] R. Long, Z. Kuang, Z. Liu, W. Liu, *J. Membr. Sci.* **2018**, *561*, 1.